

Broadband Generation of Airy Beams with Hyperbolic Metamaterials

Huihui Li, Weiming Hao, Xiang Yin, Shuqi Chen, and Lin Chen*

The Airy beam has attracted considerable research interest owing to the intriguing diffraction-free, self-accelerating, and self-healing properties, and hence has found numerous applications in photonics. Metasurfaces provide a compact method to generate Airy beams, but the available Airy beam generators suffer from the issue of narrow bandwidth since they typically rely on resonance principles. Here, hyperbolic metamaterials (HMMs) are proposed to address this issue by taking advantage of the broadband high birefringence. By changing the orientation angle of the HMM unit, the local amplitude and phase distributions of the transmitted electromagnetic waves passing through such HMM unit can be well adjusted to follow the Airy function within a wide spectral range. The resultant microwave Airy beam generator promises an operation bandwidth from 7.2 to 9.6 GHz, while the near-infrared Airy beam generator has a working bandwidth from 1.25 to 2.40 μm over 10% transmission efficiency. The proposed Airy beam overcomes the limitation of the customary Airy beams with the issue of narrow bandwidth and can stimulate the design of complicated optical devices with the requirement of maintaining the amplitude and phase distributions over a wide spectral band.

1. Introduction

The diffraction-free beams, including the Bessel beam,^[1] the Mathieu beam,^[2] and the Airy beam,^[3] have attracted increasing research interest due to their intriguing optical properties. The Airy beam is an analogy to the Airy wave packet solution for a free particle deriving from the potential-free quantum Schrödinger equation in electromagnetism.^[3–5] Benefiting from the unique diffraction-free,^[3] self-bending,^[5] and self-healing properties of the Airy beam,^[6] a number of potential applications, such as particles manipulation,^[6] light bullet,^[7,8] and curved plasma channel generation,^[9] have been stimulated. For


the generation of Airy beams, it is highly desirable to locally control the amplitude and phase of the output beam simultaneously so as to satisfy the polynary amplitude and binary phase distributions. Traditional methods to generate an Airy beam usually require a complex and bulky optical system, such as a Fourier transform (FT) lens and a spatial light modulator,^[3,6] or an FT lens and an FT plane,^[7] which is against a high-density optical integration on a chip.

Metamaterials and their 2D versions, metasurfaces, have provided an unprecedented approach to locally manipulate the phase,^[10,11] amplitude,^[12,13] and/or polarization^[14] of the electromagnetic (EM) waves. Recent studies have demonstrated that, manipulating the amplitude and phase simultaneously and independently leads to new wavefront manipulation effects and applications.^[15–17] Inspired by the flexibility of

introducing complex field distributions,^[18] various Airy beam generators, either for free-space light,^[19–25] or surface plasmons,^[20,26–30] have been proposed and demonstrated based on metasurfaces. Different from the metasurface lenses or holograms that merely require phase modulation, controlling both the amplitude and phase simultaneously is highly required to generate high-quality Airy beams that are capable of keeping good nondiffracting nature and stable full width half-maximum (FWHM) during propagation.^[23] Typically, wavelength-scale engineered gratings,^[26,29] graded nanocavity array,^[27,28] and nanoslit resonators^[20,30] are widely used to generate plasmonic Airy plasmons. In parallel with the above advances, free-space Airy beams, have been successfully realized by using dielectric nanofins,^[21] metal nanorods,^[23] and C-shaped apertures.^[19,22,24,25] All these meta-atoms provide us with a robust tool to control the wave front of output beams appreciably across a resonance, and hence can be utilized to generate Airy beams. Since the building blocks of these metasurfaces are typically some resonant structures so that the amplitude and phase cannot be kept to satisfy an Airy function at frequencies out of the resonance frequency, such schemes thus exhibit limited working bandwidths around the resonance frequency. While promising steps have been taken to broaden the working bandwidth with proper design of C-aperture metasurface, and the working bandwidth of the Airy beams can be somewhat expanded around the resonance frequency,^[22,24] the transmission efficiencies are typically low

H. Li, W. Hao, X. Yin, Prof. L. Chen
Wuhan National Laboratory for Optoelectronics
Huazhong University of Science and Technology
Wuhan 430074, China
E-mail: chen.lin@mail.hust.edu.cn

Prof. S. Chen
The Key Laboratory of Weak Light Nonlinear Photonics
Ministry of Education
School of Physics and TEDA Institute of Applied Physics
Nankai University
Tianjin 300071, China

 The ORCID identification number(s) for the author(s) of this article can be found under <https://doi.org/10.1002/adom.201900493>.

DOI: 10.1002/adom.201900493

due to the sharp reduction of transmission amplitude at frequencies far from the resonance frequency.

In recent years, the concern of metamaterial research has partially shifted to the hyperbolic metamaterials (HMMs) due to the outstanding EM properties, including the negative refraction,^[31] Purcell effect,^[32] and superlensing effects.^[33] A previous study has demonstrated that HMMs, comprised of metal–dielectric multilayer, can serve as an alternative metasurfaces that can significantly modulate the amplitude, phase and polarization of the EM waves. The amplitude and phase of transmitted EM waves can be fully controlled by a branch of spoof surface plasmons (SSPs) on the side walls of the HMMs through structural readjustment. Distinct from the plasmonic/dielectric metasurfaces that exhibit limited working bandwidth around resonance frequency, the HMM utilizes the propagation of SSPs to manipulate the amplitude and phase of the EM waves, representing an effective and robust approach to build high-efficiency broadband wave front control transmissive metadevices.^[34] While the HMMs have exhibited great capability of modulating the EM waves over a wide spectral band, generation of complex amplitude and phase distributions for realizing diffraction-free beams, such as an Airy beam, still remains unexplored.

In this paper, we demonstrate that, both of the amplitude and phase of the transmitted EM waves can be modulated by taking advantage of the broadband high birefringence of the HMM. The polynary amplitude and binary phase distributions for generating Airy beams can be simply obtained over a wide spectral range by spatially arranging the HMM meta-atoms with different orientation angles. The co-designed HMM Airy beam structures can thus present wide operating bandwidth, as demonstrated in the microwave and near-infrared domain.

2. Results and Discussions

2.1. Operating Principle

The schematic of the HMM Airy beam generator is shown in **Figure 1**, and the building block of the HMM is presented in the top right corner, consisting of a rectangle-shaped metal–dielectric multilayer on a dielectric substrate. We have previously demonstrated that such an artificial structure can always support a branch of SSP mode on both side walls,^[34] and the propagation constant of SSP mode is closely related to the cross-sectional parameters of HMM as well as the gap separation between the adjacent HMM units. An array of rectangle-shaped HMM (RHMM) offers the capability of guiding SSPs at both sides of HMM–air interfaces along the x - and y -polarization directions simultaneously. Different phase shifts can be introduced for the two orthogonal polarization directions due to the unequal SSP modes along the x - and y -polarizations. We denote the two opposing edges of the RHMM cross-section as l and s ($l \geq s$), namely the long and short sides of RHMM. The dispersion relations of SSP modes can be numerically simulated with an eigenmode solver by commercial software CST Microwave Studio. In the simulations, periodic boundary conditions are used along the x and y directions, and Bloch boundary condition is arranged along the z direction. The broadband birefringence of RHMM can be realized in any frequency regime as long as

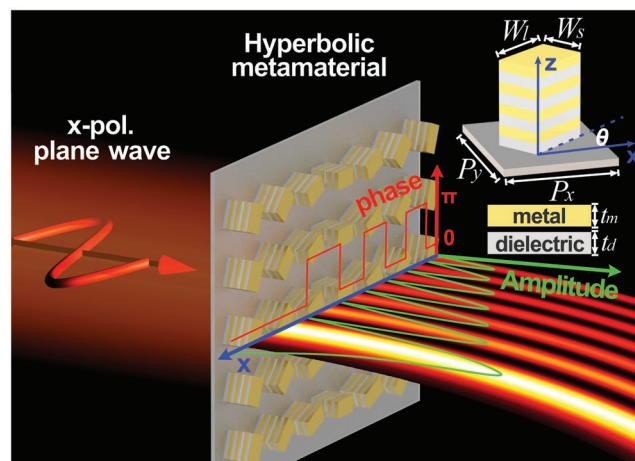


Figure 1. Schematic illustration of an Airy beam generator made of a RHMM array, where the building block of the RHMM is presented in the top right corner. The thicknesses of metal and dielectric layers are represented by t_m and t_d , respectively. The lengths of long and short axes of the RHMM unit are denoted by W_l and W_s , respectively. The orientation angle θ is defined as the angle between the x axis of laboratory coordinate and l axis.

metal–dielectric multilayer is used for building the RHMM. Here we choose the microwave regime to design the RHMM. The metal and dielectric layers are chosen as Cu (with conductivity of $5.8 \times 10^7 \Omega^{-1} \text{ m}^{-1}$ and a thickness of $t_m = 0.079 \text{ mm}$ for each layer) and FR4 (with a relative permittivity of $4.3 + 0.025j$ and a thickness of $t_d = 0.386 \text{ mm}$ for each layer), respectively. For an RHMM array with width $W_l = 8 \text{ mm}$ and $W_s = 6 \text{ mm}$ along l and s axes, transversal period $P = P_x = P_y = 13 \text{ mm}$, and longitudinal period $P_z = t_m + t_d = 0.465 \text{ mm}$, the dispersion relations of fundamental SSP modes for the two orthogonal polarization directions are shown in **Figure 2**, which clearly indicates the existence of broadband birefringence as the propagation constant for s -polarization SSP is quite different from that for l -polarization SSP within a wide spectral band. The inset of **Figure 2** shows the electric field of l -polarization SSP mainly locates at the spacing between the adjacent short edges, while that of s -polarization SSP mainly lies in the spacing between the adjacent long edges.

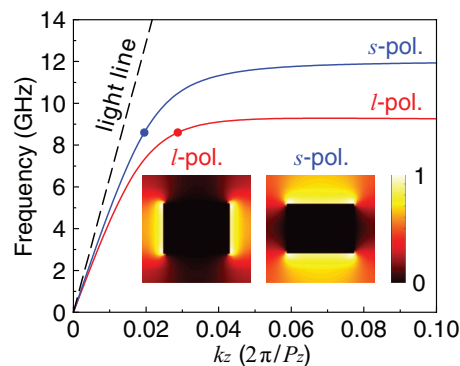


Figure 2. The dispersion relations for l - and s -polarization fundamental SSP modes of the RHMM array. The inset shows the electric field distributions for l - and s -polarization SSP modes at 8.6 GHz in the xy plane. The RHMM meta-atom is with 36 pairs of Cu/FR4 layers and 2 mm FR4 substrate.

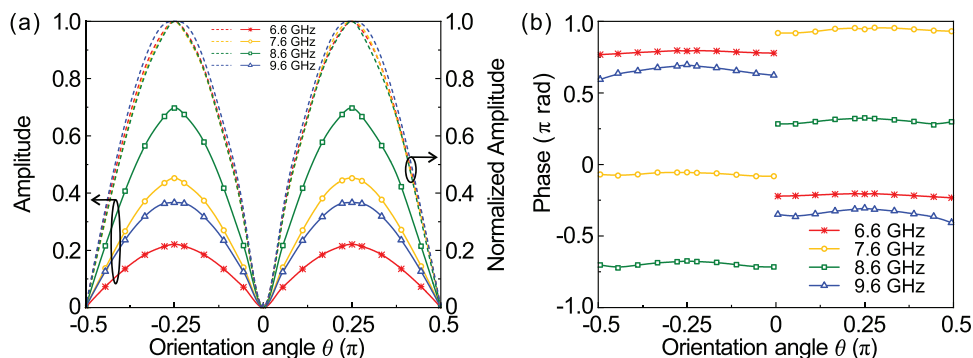


Figure 3. a) The transmission amplitude and (b) phase of γ -component electric field versus the orientation angle θ of the RHMM meta-atom for different frequencies. The normalized amplitudes for different frequencies are denoted as dashed lines in (a). The geometrical parameters of the RHMM meta-atom are the same as those in Figure 2.

Upon l - and s -polarized incidences, the complex transmission coefficients t_l and t_s can be written as

$$t_l = A_l e^{i\phi_l}, t_s = A_s e^{i\phi_s} \quad (1)$$

where A_l and A_s represent the transmission amplitude, ϕ_l and ϕ_s stand for the transmission phase along the l - and s -polarization directions, respectively. The complex transmission coefficients for any polarization direction can be obtained with a combination of t_l and t_s . Consider an RHMM meta-atom has an orientation angle θ between the x axis of laboratory coordinate and l axis (as shown in Figure 1). The unit vectors of x , y , l , and s directions are denoted by \hat{x} , \hat{y} , \hat{l} , and \hat{s} , respectively. The electric field of x -polarized EM waves with normal incidence can be expressed as $\vec{E}_i = E_i \cdot \hat{x}$, where E_i represents the amplitude. The γ -component electric field of transmitted EM waves is obtained by vector decomposition and synthesis of electric field along the l and s directions (see Note S1 in the Supporting Information), and can be written as

$$\vec{E}_{i,\gamma} = \frac{1}{2} E_i (A_l e^{i\phi_l} - A_s e^{i\phi_s}) \sin(2\theta) \hat{y} = \begin{cases} \frac{1}{2} E_i C |\sin(2\theta)| e^{i\chi+\pi} \hat{y}, & \theta \in [-\pi/2, 0) \\ \frac{1}{2} E_i C |\sin(2\theta)| e^{i\chi} \hat{y}, & \theta \in [0, \pi/2) \end{cases} \quad (2)$$

where C and χ are the modulus and argument of complex value $(A_l e^{i\phi_l} - A_s e^{i\phi_s})$, respectively. Our aim is to use the RHMM to simultaneously control the amplitude and phase of γ -component electric field of the transmitted waves so as to generate broadband Airy beams. According to Equation (2), the local amplitude of γ -component electric field is $\frac{1}{2} E_i C |\sin(2\theta)|$. It can easily be inferred that, the local amplitude of γ -component electric field is solely associated with θ once the RHMM has a certain geometry. Meanwhile, when light frequency is deviated from predesigned frequency, the local amplitude of γ -component electric field is changed since C is frequency-dependent, but the normalized amplitude, $|\sin(2\theta)|$, is almost unchanged. The local phase of γ -component electric field is $(\chi+\pi)$ with $\theta \in [-\pi/2, 0)$ and χ with $\theta \in [0, \pi/2)$. This indicates that, the local phase of γ -component electric field is kept constant as θ is varied from $-\pi/2$ to 0, but undergoes a phase shift of π as θ ranges from 0 to $\pi/2$. As light frequency is deviated from

predesigned frequency, the local phase of γ -component electric field suffers from a phase shift of π as θ changes from $[-\pi/2, 0)$ to $[0, \pi/2)$, although χ is frequency-dependent. To briefly conclude here, for a certain geometry of an RHMM, the normalized amplitude (equal to $|\sin(2\theta)|$) does not change with light frequency, and the local phase always experiences a phase shift of π as θ changes from $[-\pi/2, 0)$ to $[0, \pi/2)$, regardless of light frequency. The presented strategy of generating amplitude and phase is thus applicable to the design of Airy beam generators over a wide spectral bandwidth in principle, so long as operation frequency is below the cutoff frequency of SSP mode with s -polarized incidence (11.9 GHz; Figure 2).

To validate the above prediction, the finite difference time domain (FDTD) method by commercial software Lumerical FDTD Solutions is performed to model the EM response of an RHMM array. Periodic boundary conditions are employed in the x and y directions, and perfectly matched layer (PML) absorption boundary condition is applied in the z direction. The simulation results shown in Figure 3 clearly reveal that the transmission amplitude of γ -component electric field can be modulated over a wide range by tuning θ . The amplitude distributions versus θ are different for different frequencies, but the normalized amplitude distributions for different frequencies are essentially coincident, which agrees with the above conclusion that the normalized amplitude for an RHMM meta-atom does not change with light frequency. In addition, the phase distributions versus θ for different frequencies all present approximate π phase shift as θ changes from $[-\pi/2, 0)$ to $[0, \pi/2)$.

It is important to discuss the factors that affect the absolute transmission amplitude of an RHMM meta-atom, which will finally determine the transmission efficiency of designed devices. Although the RHMM meta-atom can work in transmission mode as light frequency is below the cutoff frequency of SSP mode with s -polarized incidence (11.9 GHz, as shown in Figure 2), C is significantly influenced by the birefringence index. When light frequency is low, C is very small as ϕ_l and ϕ_s are close due to the small birefringence index. Benefiting from the enhanced birefringence as frequency increases, C is thus increased. As frequency is further increased and approaches the cutoff frequency, C will decrease significantly due to the sharp reduction of A_l and A_s . To briefly conclude here, although

the RHMM can keep the normalized amplitude and phase shift over a wide spectral band, the transmission efficiency can be distinct for different frequencies.

2.2. Design, Fabrication, and Measurement of HMM Airy Beam Generator

By spatially arranging an array of RHMM units, with the orientation angle θ being different along the x direction to enable $\vec{E}_{t,y}$ of the transmitted EM waves to satisfy the initial envelope of the Airy beam, y -polarized Airy beam generators under the x -polarized incidence can be designed (as shown in Figure 1). The electric field envelope of a finite energy 1D Airy beam is described as follows^[21]

$$U(\rho, \gamma) = A \cdot \text{Ai} \left[\gamma - \left(\frac{\rho}{2} \right)^2 + j(\alpha\rho) \right] \exp \left[\alpha\gamma - \left(\frac{\alpha\rho^2}{2} \right) - j \left(\frac{\rho^3}{12} \right) + j \left(\frac{\alpha^2\rho}{2} \right) + j \left(\frac{\gamma\rho}{2} \right) \right] \quad (3)$$

where A and Ai represent the amplitude factor of electric field and Airy function, respectively, and the exponential term indicates the decaying feature. The parameter α is the decay factor, and $\gamma = (x - x_0)/w$ is the normalized dimensionless transverse coordinate, where x is the real laboratory coordinate, x_0 is the reference coordinate for normalization, and w represents the scaling length. $\rho = z/(k_0 w^2)$ is the propagation length normalized with Rayleigh distance, where k_0 is the wave number in free space. The initial field envelope of the Airy beam with the condition of $\rho = 0$ is given as

$$U_0(x) = U(0, x) = A \cdot \text{Ai} \left(\frac{x - x_0}{w} \right) \exp \left[\alpha \left(\frac{x - x_0}{w} \right) \right] \quad (4)$$

where $U_0(x)$ is a real-value function, depending on the imparted amplitude and phase. A positive and negative value of $U_0(x)$ requires a phase modulation of χ and $(\chi + \pi)$, respectively. For designing a broadband Airy beam generator, Equation (4) should be rewritten with the involvement of the operating frequency f

$$U_0(f, x) = A(f) \cdot \text{Ai} \left(\frac{x - x_0}{w} \right) \exp \left[\alpha \left(\frac{x - x_0}{w} \right) \right] \quad (5)$$

To guarantee the maximum transmission efficiency of the Airy beam generator at the designed frequency of f_0 , $A(f_0)$ should be properly selected to satisfy $|U_0(f_0, x)|_{\max} = \frac{1}{2} C(f_0) E_i$. $A(f_0)$ is 0.76 at $f_0 = 9.1$ GHz. Specifically, $\alpha = 0.01$, $w = P/0.3$ and $x_0 = 43.55$ cm are used to construct the Airy beam generators. 47 RHMM units are placed along the x direction with equidistant sampling, while they are assumed to be uniform and sufficiently long along the y direction. The orientation angle θ for each RHMM unit along the x direction can be found in Table S1 of Note S2 in the Supporting Information.

Figure 4a presents the Airy beam profile, where the red circles represent the samplings. FDTD simulation is used to predict the performance of the HMM Airy beam generator.

In the simulations, PML absorption boundary conditions are employed in the x and z directions, and periodic boundary condition is applied in the y direction. A part of the sample is schematically shown in Figure 4b, and the detailed preparation process and the experimental measurement setup can be found in Note S3 in the Supporting Information. The field distributions in the near-field zone were measured via a vector network analyzer, where the distance between the source and the sample is 250 cm. The field intensity distributions at 9.1 GHz shown in Figure 4c,d clearly indicate that, Airy beams are generated under the x -polarized incidence, and the simulated and experimental results are basically consistent. More field intensity distributions are shown in Figures S3 and S4 of Note S4 in the Supporting Information, suggesting high-quality envelope was generated from 7.2 to 9.6 GHz. Although broadband generation of Airy beams with the RHMM is feasible, their spatial intensity distributions are wavelength-dependent, which is consistent with that predicted by Equation (3). This is different from a recent work on using specifically designed dielectric metasurfaces to generate Bessel beams, where the transverse intensity profiles are wavelength-independent.^[35] It is worth mentioning that, because of essential amplitude modulation, the ideal efficiency of the designed Airy beam generator is 24% considering the case when $\gamma \in (-10, 4)$ and $\alpha = 0.01$. The ideal efficiency was defined by the ratio of the power of the Airy beam divided by input power. To emphasize the contrast of the Airy beam rather than its power, we define a transmission efficiency as the ratio of the maximum electric field intensity of Airy beam to the intensity of incident plane wave. This definition is widely used in the references of the Airy beam study.^[22,36] The transmission efficiency for the present Airy beam generator firstly increases with frequency, but reduces with frequency after it reaches the maximum value of 30% at 8.2 GHz (Figure 4e). The variable transmission efficiency with frequency can be attributed to frequency-dependent birefringence, as discussed in the above section. It should be noted here, although the presented Airy beam generator can work over an wide spectral band below the cutoff frequency of SSP mode with s -polarized incidence, the experimental results merely show the broadband properties within 7.6–9.6 GHz, basically consistent with the simulated operation bandwidth.

Self-bending, diffraction-free, and self-healing features are three fascinating optical properties of the Airy beam. The former two features can be evaluated by deflection offset of main lobe, x_d , and the FWHM, respectively. Under the paraxial approximation, the theoretical value of deflection offset, x_d , can be described as^[3]

$$x_d \approx \lambda^2 z^2 / (16\pi^2 w^3) \quad (6)$$

The simulated and experimental results for deflection offset at 9.1 GHz in Figure 5a are almost the same as the estimated value from Equation (6). The FWHM is oscillating around the predesigned value of 7.06 cm when the propagation distance is below 120 cm (around 36-fold wavelengths), and is enhanced sharply as the propagation distance is above 120 cm due to the gradual degradation of beam quality with propagation (Figure 5b). The self-healing feature is typically verified by placing a scatterer on the travelling path of the main lobe.

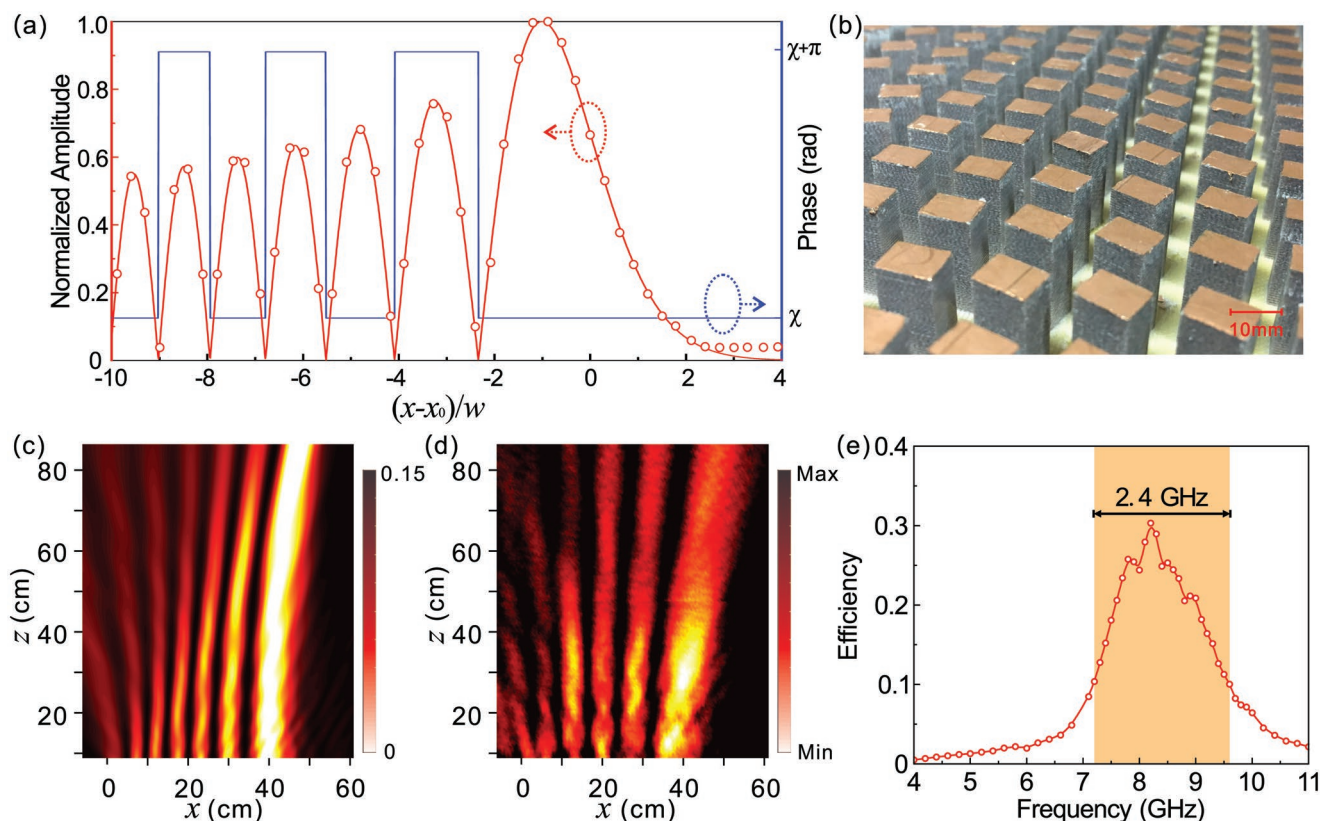


Figure 4. Design and verification of the broadband HMM Airy beam generator. a) The normalized amplitude profile: red solid line for an ideal Airy beam and red hollow circles for sampling points. The blue solid line represents the phase profile. b) A part of the fabricated sample. The field intensity distributions of output fields of the sample by (c) full-wave simulation and (d) experiment at 9.1 GHz. e) The transmission efficiency as a function of frequency.

The main lobe can recover quickly if a perfect electric conductor with $4 \text{ cm} \times 6 \text{ cm}$ in size is located at $(x, z) = (-4 \text{ cm}, 20 \text{ cm})$, presenting rather robust self-healing property of the generated Airy beam (Figure 5c). The broadband properties of self-bending, diffraction-free, and self-healing features can be found in Note S5 in the Supporting Information. The deviation of the field pattern between the simulated and measured results mainly comes from the near-field scanning measurement,

including the imperfect wave front of incident waves illuminating upon the sample, wave diffraction, and the scattering effect arising from the probe and the cable connecting the probe with the vector network analyzer (see more analysis on measurement error in Note S6 in the Supporting Information).

The design strategy of the broadband Airy beam generator can also be extended to terahertz and optical frequency range. We also choose to demonstrate RHMM Airy beam generator

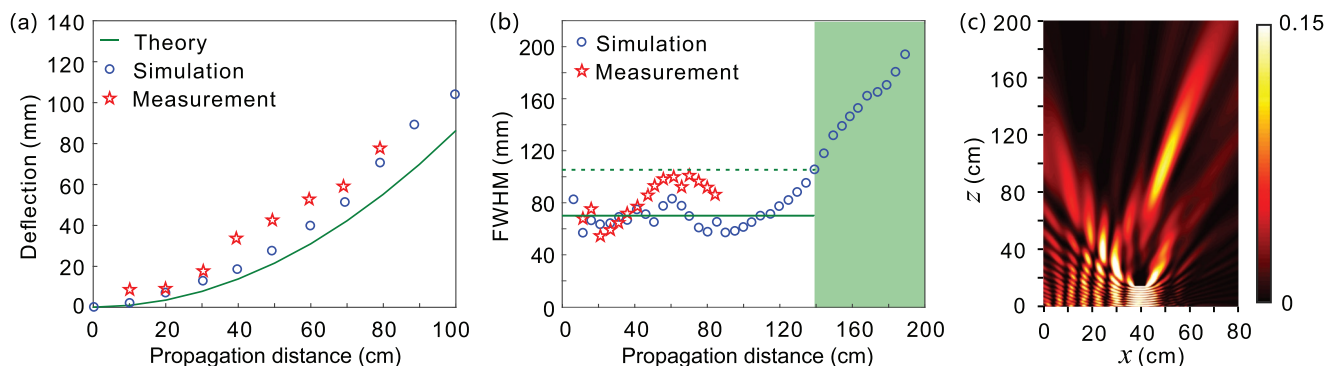


Figure 5. The self-bending, diffraction-free, and self-healing features of the Airy beam at 9.1 GHz. a) The self-bending feature is characterized by deflection offset of the main lobe. The green line, hollow circles, and red pentagrams represent the deflection offset of the main lobe derived from Equation (6), full-wave simulation, and experimental measurement, respectively. b) The FWHM of the main lobe versus the propagation distance. The nondiffracting zone is defined as the region, where the FWHM is below 1.5 times of the predefined values (green dashed line). The green shadow region represents the diffracting zone. c) The field intensity distribution after placing a perfect electric conductor with $4 \text{ cm} \times 6 \text{ cm}$ in size located at $(x, z) = (-4 \text{ cm}, 20 \text{ cm})$, on the path of the main lobe.

in the near-infrared range as the huge Ohmic loss of metal contributes to the final transmission efficiency (see more details in Note S7 in the Supporting Information). To experimentally implement the RHMM in the optical regime, the metal/dielectric multilayer can be precisely prepared by deposition techniques such as electron beam evaporation or magnetron sputtering deposition. The pattern of RHMM array can be finally formed with etching techniques such as reactive ion etching or focused ion-beam milling.^[37–39] We have made fabrication-tolerance analysis with numerical simulations, and the presented results demonstrate that the generation of broadband Airy beams is rather robust to thickness error for each metal/dielectric layer and taper-like sidewalls (see more details regarding of fabrication-tolerance analysis in Note S8 in the Supporting Information). Compared with the Airy beam generators with single-layer metasurfaces, the presented HMM one has the advantage of generating Airy beams over a wide spectral band, while the transmissions efficiency is comparable (see more comparison as listed in Table S3 of Note S9 in the Supporting Information).

3. Conclusion

To sum up, we have proposed a general strategy for generating a broadband Airy beam with RHMM metasurfaces. Inspired by the high birefringence over a wide spectral range, the RHMM can overcome bandwidth limitation of the customary Airy beam generators with plasmonic/dielectric metasurfaces. By changing the orientation angle of the RHMM unit, the local amplitude and phase distributions of the transmissive EM waves can be well adjusted to follow the Airy function over a wide spectral range. We have demonstrated the broadband generation of high-efficiency Airy beams in the microwave/infrared regimes. Our results can stimulate constructing broadband and complicated optical devices, with the requirement to maintain the amplitude and phase distributions simultaneously over a wide spectral band.

Supporting Information

Supporting Information is available from the Wiley Online Library or from the author.

Acknowledgements

The authors thank Tao Xu and Zhi Hong Hang from Soochow University for the experimental assistance. This work was supported by the National Natural Science Foundation of China (Grant Nos. 11474116 and 11674118) and the State Key Laboratory of Advanced Technology for Materials Synthesis and Processing (Wuhan University of Technology).

Conflict of Interest

The authors declare no conflict of interest.

Keywords

Airy beams, broadband, hyperbolic metamaterials

Received: March 20, 2019

Revised: July 10, 2019

Published online:

- [1] J. Durnin, J. J. Miceli, J. H. Eberly, *Phys. Rev. Lett.* **1987**, *58*, 1499.
- [2] J. C. Gutiérrez-Vega, M. D. Iturbe-Castillo, S. Chávez-Cerda, *Opt. Lett.* **2000**, *25*, 1493.
- [3] G. A. Siviloglou, J. Broky, A. Dogariu, D. N. Christodoulides, *Phys. Rev. Lett.* **2007**, *99*, 213901.
- [4] M. V. Berry, N. L. Balazs, *Am. J. Phys.* **1979**, *47*, 264.
- [5] G. A. Siviloglou, D. N. Christodoulides, *Opt. Lett.* **2007**, *32*, 979.
- [6] J. Baumgartl, M. Mazilu, K. Dholakia, *Nat. Photonics* **2008**, *2*, 675.
- [7] P. Panagiotopoulos, D. G. Papazoglou, A. Couairon, S. Tzortzakos, *Nat. Commun.* **2013**, *4*, 2622.
- [8] D. Abdollahpour, S. Sunstov, D. G. Papazoglou, S. Tzortzakos, *Phys. Rev. Lett.* **2010**, *105*, 253901.
- [9] P. Polynkin, M. Kolesik, J. V. Moloney, G. A. Siviloglou, D. N. Christodoulides, *Science* **2009**, *324*, 229.
- [10] N. Yu, P. Genevet, M. A. Kats, F. Aieta, J.-P. Tetienne, F. Capasso, Z. Gaburro, *Science* **2011**, *334*, 333.
- [11] T. Yang, H. Lin, B. Jia, *Front. Optoelectron.* **2018**, *11*, 2.
- [12] M. A. Kats, D. Sharma, J. Lin, P. Genevet, R. Blanchard, Z. Yang, M. M. Qazilbash, D. N. Basov, S. Ramanathan, F. Capasso, *Appl. Phys. Lett.* **2012**, *101*, 221101.
- [13] X. Kong, J. Xu, J.-j. Mo, S. Liu, *Front. Optoelectron.* **2017**, *10*, 124.
- [14] J. K. Gansel, M. Thiel, M. S. Rill, M. Decker, K. Bade, V. Saile, G. von Freymann, S. Linden, M. Wegener, *Science* **2009**, *325*, 1513.
- [15] S. Divitt, W. Zhu, C. Zhang, H. J. Lezec, A. Agrawal, *Science* **2019**, *364*, 890.
- [16] A. C. Overvig, S. Shrestha, S. C. Malek, M. Lu, A. Stein, C. Zheng, N. Yu, arXiv:1903.00578, **2019**.
- [17] G. Y. Lee, G. Yoon, S. Y. Lee, H. Yun, J. Cho, K. Lee, H. Kim, J. Rho, B. Lee, *Nanoscale* **2018**, *10*, 4237.
- [18] H.-T. Chen, A. J. Taylor, N. Yu, *Rep. Prog. Phys.* **2016**, *79*, 076401.
- [19] J. He, S. Wang, Z. Xie, J. Ye, X. Wang, Q. Kan, Y. Zhang, *Opt. Lett.* **2016**, *41*, 2787.
- [20] S. Wang, X. Wang, Y. Zhang, *Opt. Express* **2017**, *25*, 23589.
- [21] Q. Fan, D. Wang, P. Huo, Z. Zhang, Y. Liang, T. Xu, *Opt. Express* **2017**, *25*, 9285.
- [22] E. Y. Song, G. Y. Lee, H. Park, K. Lee, J. Kim, J. Hong, H. Kim, B. Lee, *Adv. Opt. Mater.* **2017**, *5*, 1601028.
- [23] Z. Li, H. Cheng, Z. Liu, S. Chen, J. Tian, *Adv. Opt. Mater.* **2016**, *4*, 1230.
- [24] J. Ding, S. An, B. Zheng, H. Zhang, *Adv. Opt. Mater.* **2017**, *5*, 1700079.
- [25] S. Keren-Zur, O. Avayu, L. Michaeli, T. Ellenbogen, *ACS Photonics* **2016**, *3*, 117.
- [26] A. Minovich, A. E. Klein, N. Janunts, T. Pertsch, D. N. Neshev, Y. S. Kivshar, *Phys. Rev. Lett.* **2011**, *107*, 116802.
- [27] L. Li, T. Li, S. M. Wang, S. N. Zhu, *Phys. Rev. Lett.* **2013**, *110*, 046807.
- [28] L. Li, T. Li, S. M. Wang, C. Zhang, S. N. Zhu, *Phys. Rev. Lett.* **2011**, *107*, 126804.
- [29] C. Guan, T. Yuan, R. Chu, Y. Shen, Z. Zhu, J. Shi, P. Li, L. Yuan, G. Brambilla, *Opt. Lett.* **2017**, *42*, 563.
- [30] X. Yin, L. Chen, X. Li, *Opt. Express* **2018**, *26*, 23251.
- [31] R. A. Shelby, D. R. Smith, S. Schultz, *Science* **2001**, *292*, 77.
- [32] Z. Jacob, I. I. Smolyaninov, E. E. Narimanov, *Appl. Phys. Lett.* **2012**, *100*, 181105.
- [33] Z. Liu, H. Lee, Y. Xiong, C. Sun, X. Zhang, *Science* **2007**, *315*, 1686.

- [34] X. Yin, H. Zhu, H. Guo, M. Deng, T. Xu, Z. Gong, X. Li, Z. H. Hang, C. Wu, H. Li, S. Chen, L. Zhou, L. Chen, *Laser Photonics Rev.* **2019**, *13*, 1800081.
- [35] W. T. Chen, M. Khorasaninejad, A. Y. Zhu, J. Oh, R. C. Devlin, A. Zaidi, F. Capasso, *Light: Sci. Appl.* **2017**, *6*, e16259.
- [36] W. Hao, M. Deng, S. Chen, L. Chen, *Phys. Rev. Appl.* **2019**, *11*, 054012.
- [37] D. Lu, J. J. Kan, E. E. Fullerton, Z. Liu, *Nat. Nanotechnol.* **2014**, *9*, 48.
- [38] J. Valentine, S. Zhang, T. Zentgraf, E. Ulin-Avila, D. A. Genov, G. Bartal, X. Zhang, *Nature* **2008**, *455*, 376.
- [39] S. S. Kruk, Z. J. Wong, E. Pshenay-Severin, K. O'Brien, D. N. Neshev, Y. S. Kivshar, X. Zhang, *Nat. Commun.* **2016**, *7*, 11329.